Propagation effects in the assessment of laser damage thresholds to the eye and skin

Robert J. Thomas,[c] Rebecca L. Vincelette,[a] C.D. Clark III,[b]
Jacob Stolarski,[a] Lance J. Irvin[c] and Gavin D. Buffington[c]

[a] Air Force Research Laboratory, 2624 Louis Bauer Drive, San Antonio, TX, USA 78325
[b] Northrop Grumman, 4241 Woodcock Dr. Ste B-100, San Antonio, TX, USA 78228
[c] Fort Hays State University, 600 Park St., Hays, KS, USA 67601

ABSTRACT

Computational physics methods are described for the evaluation of the role of propagation with regard to laser damage to tissues. Regions of the optical spectrum, where linear and non-linear propagation affects irradiance distributions within tissues, are examined. Effects described include group-velocity dispersion, aberrations, thermal lensing, and self-focusing. Implications to exposure limits within safety standards, incorporating these irradiance-altering effects, are addressed such that inherent trends agree over wide temporal and spectral ranges, with damage thresholds measured experimentally. We present current regions of interest to the standard-setting community and recent works showing how propagation effects may be playing a key role in assessing damage thresholds.

Keywords: laser damage, laser-tissue interaction, computational physics, beam propagation, heat transfer

1. INTRODUCTION

The establishment of exposure limits for laser safety has been an active research field since the advent of the laser itself.[1] Throughout the history of laser safety standards, such as the ANSI Z136.1 American National Standard for Safe Use of Lasers[2] (first adopted in 1973), researchers have attempted to reflect the best knowledge to date of dosimetry and damage mechanisms. These have included photo-thermal, photo-mechanical, laser-induced breakdown (LIB) or ionization damage as well as photo-chemical toxicity.

Exposure limits commonly address skin and eye hazards through separate definitions. Differing optical absorption and scattering properties, as well as the focusing optics of the eye, create a variety of distributions of irradiance within the tissue. Trends in exposure limits, as a function of the exposure time and optical wavelength, attempt to empirically describe the mechanisms at play. For example, the exposure limit for the retina transitions from a time-dependent to a time-independent value in terms of radiant exposure as times shorten below thermal confinement limits.

The current exposure-limit definitions take into account some propagation effects due to the nature of the available experimental data used in their creation. For example, retinal exposure limits derived from experimental damage thresholds include the chromatic aberrations (chromatic defocus) of the eye. In the common *in-vivo* experiment, a collimated beam is delivered to an emmetropic eye, which would produce a sharp focus for visible wavelengths. An infrared beam, however, is defocused at the retina, changing the irradiance and increasing the damage threshold to the retina. As limits are defined for exposure levels at the cornea, one can see an increase in the exposure limit with wavelength, partially attributed to this chromatic defocus, and partially due to increasing pre-retinal absorption.

Recently, our interest has been in determining spectral, temporal, spatial, and amplitude parameters for which propagation effects may play a role in determining retinal damage thresholds.[3,4] In particular, we have examined regions where the common experimental configuration of a collimated beam at a single beam diameter does not represent the highest risk to those exposed. Our research has led us to a few specific hypotheses, two of which are described here. One is the case of ultrafast-pulsed laser exposures. Here, our hypothesis is that group-velocity dispersion (GVD) significantly broadens a pulse along the propagation length within the eye.

Optical Interactions with Tissue and Cells XVIII, edited by Steven L. Jacques, William P. Roach,
Proc. of SPIE Vol. 6435, 64350A, (2007) · 1605-7422/07/$18 · doi: 10.1117/12.715190

The consequence of this hypothesis, if true, is that a pulse-chirp compensation system (now common to the laboratory) may counteract this GVD effect and reduce thresholds for damage to the retina.

The second hypothesis recently examined is that the extremely large laser damage thresholds for the retina found near 1320 nm for long-pulse exposures[5] are actually the consequence of thermal lensing within the eye. In this wavelength region, absorption coefficients for the pre-retinal portions of the eye (see Figure 1) are such that energy is absorbed over the entire axial length. The importance of this hypothesis to laser safety is that the empirical trends in exposure limits currently under consideration may not correctly account for the parameters relevant to the minimal damage threshold with thermal lensing. That is, beam diameters used in the experiments may affect the magnitude of the thermal lens, and therefore do not represent the minimal damage threshold as a function of pupil size. In addition, the limited numbers of data points available do not sufficiently represent or capture the rise-time of the thermal lens, leading to improper exposure limits as a function of exposure duration.

Here, we describe theoretical and computational methods which have been used to evaluate the validity of our hypothesis and understand the experimental data available. Below, the hypotheses described above are examined in some detail in the context of these methods.

2. METHODS

2.1. Ultrafast-Pulse Models

Laser-induced breakdown has been implicated in the threshold for damage of the retina for pulse durations below 100 fs.[3,6,7] This pulse duration also is the lower bound for currently established laser exposure limits,[2] even though lasers with temporal pulse widths in the 10-100 fs range are becoming more common. We have theoretically assessed the dependence of the LIB threshold propagation in the eye in the wavelength band relevant for retinal damage (400 to 1400 nm). Of interest are both aberrations and GVD, including allowances for changes in the input pulse chirp. With such models, trends in retinal damage can be predicted to determine if and how extension of the 1 ps to 100 fs maximum permissible exposure levels can provide significant protection from lasers with sub-100-fs duration.For most pulse durations LIB occurs in the eye well above the threshold for minimal (first ophthalmoscopically detected, single pulse) retinal damage.

In an attempt to understand the trends in energy required to create LIB, and therefore threshold levels for retinal damage, we have extensively investigated and reported LIB thresholds in an artificial eye and *in vivo* for many pulse durations, as short as 40 fs in duration.[3] Laser pulse durations between 5 fs and 50 fs are dramatically affected during propagation through homogeneous optical materials by a number of linear and nonlinear phenomena, and which in turn influence peak irradiances acheived experimentally. A significant linear effect is GVD. Because of this, we have pursued the characterization of ocular components as part of our research program. For example, Figure 2 shows the typical change in refractive index with wavelength (dispersion) for vitreous humor, taken from Hammer et al.[8]

The bandwidth of a femtosecond pulse is inversely related to the pulse duration. To capture the relative values of the bandwidth for ultrashort pulses, one must evaluate the following relationship between minimum pulse duration and minimum wavelength bandwidth:

$$\Delta\tau_{fwhm}\Delta\lambda_{fwhm} = \frac{2\lambda^2}{\pi\, c}\ln 2 = \frac{0.4413}{c}\lambda^2 \tag{1}$$

Here $\Delta\tau_{fwhm}$ is the pulse duration, $\Delta\lambda_{fwhm}$ is the bandwidth, c is the speed of light, and λ is the center wavelength. A typical bandwidth for a 20-fs, 800-nm pulse is 47 nm, meaning that the (minimum) wavelength range for such a pulse is 776 – 824 nm. As can be seen in Figure 2, the refractive index is different across this wavelength range, such that the speed of light for the different wavelengths changes. Because of this, the red end of the pulse will travel faster than the blue end of the pulse, spreading it as it propagates.

Cain, *et al.*[3] showed that by appropriately preparing a 40-fs pulse, the LIB threshold could be changed at the focus of an artificial eye.[10] The threshold for LIB was reduced from 0.29 μJ to 0.19 μJ when the phase was correctly compensated to create the shortest pulse duration as it neared the focus. More importantly, they also measured a similar reduction in the retinal damage threshold from 0.25 to 0.17 μJ with a chirp compensation.

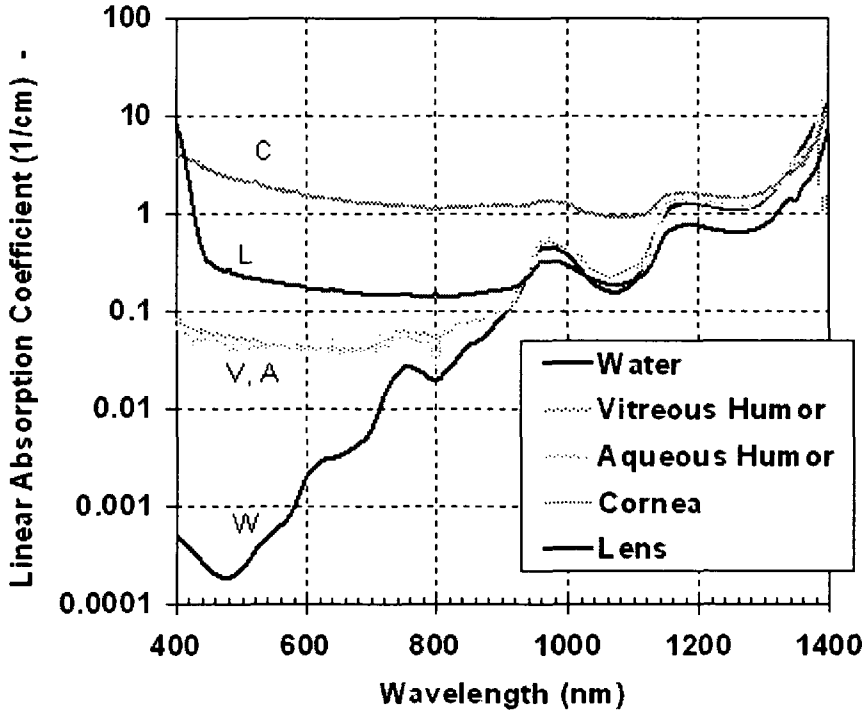

Figure 1. Absorption properties of the pre-retinal portions of the eye and water, after Maier.[9]

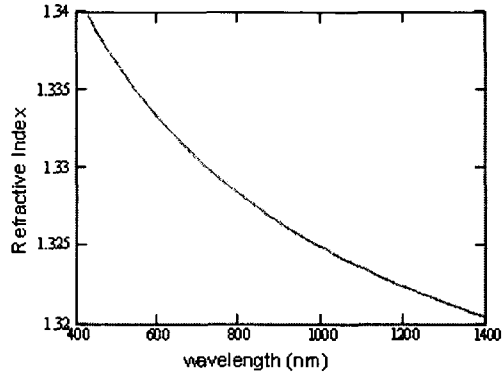

Figure 2. Refractive index variation of vitreous humor in the retinal hazard spectral region.

In order to understand these results, we have implemented a method for extending the experimental and modeling results of Cain, *et al.*[3] to the full range of wavelengths and pulse durations relevant for retinal damage. We have also demonstrated improved modeling for absolute values of predicted damage threshold versus relative threshold values. We have extended our modeling parameters to address two experimental conditions (the rhesus eye and the Cain artificial eye),[10] and a condition most relevant for laser safety, the human eye.

Applying the hypothesis that LIB leads to threshold retinal damage for pulses of less than about 100-fs duration, we scale the computed peak irradiance to predict input pulse energy for damage. The LIB threshold is affected by the peak irradiance achieved within the focal volume of the system and therefore by the linear chirp of the input beam. We search the modeling results for the lowest LIB threshold for each wavelength and pulse duration combination (the conservative safety analysis). We calculate the trends expected for LIB as the input pulse chirp is altered. From these computations we should be able to predict damage threshold to the retina as a function of a number of parameters including wavelength, beam size entering the eye, type of eye, aberration parameters, pulse chirp, and pulse duration.

To characterize the behavior of femtosecond laser pulses in the focal region of the eye, we employed a procedure described in the literature on the subject published by Kempe and Rudolph.[11] The spatial and temporal properties of the electric field U(v,u,t) can be described by Equation 2.

$$
\begin{aligned}
U(v,u;t) \propto \int_{-\infty}^{\infty} d(\Delta\omega)\,\beta(\Delta\omega) \int_0^1 dr\; r\; J_0\left[rv\left(1+\frac{\Delta\omega}{\omega}\right)\right] \\
exp\left(-r^2\right) exp\left(-iur^2/2\right) exp\left(-iAr^4\right) exp\left[-i\Psi\left(\Delta\omega, r\right)\right] \\
exp\left\{-i(\Delta\omega)\left[t+\tau\left(\Delta\omega, r\right)r^2+\frac{r^2u}{2\omega_0}\right]\right\}
\end{aligned}
\tag{2}
$$

Here, we have applied normalized optical coordinates $v = ak_0r'/z$, and $u = a^2k_0(1/f_0 - 1/z)$ where z is the distance from the lens with $u = 0$ at the focal length, and r' is the radius coordinate in an observation plane perpendicular to the optical axis. The symbol a is used to represent the entrance pupil radius. In Equation 2, $\beta(\Delta\omega)$ is the spectral amplitude of the input pulse at a frequency $\Delta\omega = \omega - \omega_0$. The term containing $exp(-iAr^4)$ represents the spherical aberration of the system, and the term containing $exp\left[-i\Psi\left(\Delta\omega, r\right)\right]$ contains the effects of GVD path difference and other chromatic aberrations, combined for our system focusing into a dispersive medium. This term is perhaps the most significant change from the previous models, which do not include the dispersive nature and aberrations, related to the target medium, which has typically been modeled as a vacuum.

Analysis includes combining Equation 2 with fitted parametric functions for optical path difference as a function of wavelength to characterize aberrations. The results incorporate temporal, chromatic, and spherical effects as outlined in our previous work.[3] The resulting irradiance profile was normalized to a known pulse energy and values were computed for beam diameter, and pulse duration from second moment integrals. These values were in turn fed to the LIB model of Kennedy[12] which provided the absolute value of LIB threshold for the computation. Parameters for the computation, as well as the strategy for numerical analysis, are documented elsewhere.[3]

This model includes a search for the circle of least confusion near the focus of the optic. For the mild aberrations exhibited for the Cain artificial eye and the values which were assumed for moderate common aberrations for the human and rhesus eye, the shift from the anticipated focal position was not significant. The differences in peak irradiance were found to be significant, however, and altered the conclusions of our study from early assumptions regarding the focal point. For all cases the LIB threshold was estimated at this optimal location for peak irradiance and consequently, minimal LIB threshold.

2.2. Continuous-Wave Models

Our second case of a method for analyzing effects of propagation on laser damage thresholds is to incorporate a full propagation method for a laser beam in the eye, and then link this propagation to a heat-transfer code and subsequent damage model. This can be accomplished through the beam propagation methods presented by

Kovsh et al[13] in the assessment of optical limiters. The procedure consists of employing one of the recent finite-difference beam propagation methods (FD-BPMs) to predict the irradiance distribution of a beam propagating in a linear or non-linear liquid.

The propagation method uses, as a starting point, a solution to the Helmholtz Equation for a propagating scalar electric field $\Psi(z,r)$. We have applied the Fresnel approximation of the Helmholtz Equation:

$$i\frac{\partial\Psi}{\partial z} = \frac{-1}{2k\bar{n}}\left[\frac{\partial^2}{\partial r^2} + \frac{1}{r}\frac{\partial}{\partial r} + k^2\left[n^2(r,z) - \bar{n}^2\right]\right]\Psi \tag{3}$$

$$i\frac{\partial\Psi}{\partial z} = \hat{S}\Psi(z) \tag{4}$$

where the operator $\hat{S}$ is defined as:

$$\hat{S} = \frac{-1}{2k\bar{n}}\left[\frac{\partial^2}{\partial r^2} + \frac{1}{r}\frac{\partial}{\partial r} + k^2\left[n^2(r,z) - \bar{n}^2\right]\right] \tag{5}$$

with a special representation at $r = 0$, below, applying the boundary condition of a vanishing first derivative of the electric field, and an assessment of the resultant indeterminate form.

$$\hat{S} = \frac{1}{2k}\left[\frac{\partial^2}{\partial r^2} + k^2\left[n^2(r,z) - \bar{n}^2\right]\right] \tag{6}$$

Application of this form of the $\hat{S}$ operator provides the following representation of a solution from an initial electric field distribution, propagated from a coordinate z to $z + \Delta z$.

$$\Psi(r, z + \Delta z) = exp\left(-iz\hat{S}\right)\Psi(r,z) \tag{7}$$

Solutions of Equation 7 include Caley's Method[14] (a Crank-Nicholson method), and solutions employing Pade operators.[15] These time-independent solutions can be coded with finite-difference methods and used to compute the irrandiance within a material at any point.

Consider the case of simple thermal lensing. The value of $n(z,r)$ becomes a function of the local temperature within the material. A water-like material will exhibit a reduction in refractive index with increasing temperature. A laser beam with a Gaussian spatial distribution will consequently create a refractive index gradient as it heats a material in which it propagates. The temperature distribution can be determined through the use of a two-dimensional, heat-transfer equation in cylindrical coordinates (given by Equation 8) with a source term (defined by Equation 9). This refractive index gradient will act as a diverging lens and cause the beam to broaden as it propagates.

$$\rho c\frac{\partial\nu}{\partial t} = \frac{\kappa}{r}\frac{\partial\nu}{\partial r} + \frac{\partial}{\partial r}\left(\kappa\frac{\partial\nu}{\partial r}\right) + \frac{\partial}{\partial z}\left(\kappa\frac{\partial\nu}{\partial z}\right) + A(z,r;t) \tag{8}$$

$$A(z,r,t) = h(z,r)H_0(\lambda,t)\mu_a(z,\lambda) \tag{9}$$

This source term provides a time-dependent description of the linear absorption of optical energy as a function of depth in the tissue, complete with spectral and radial dependence of energy being absorbed. The variable λ refers to the wavelength of the THz source. The function, $h(z,r)$, specifies the relative irradiance for a given position in the cylindrical coordinate system and includes losses due to linear absorption. This term also addresses the focusing of the beam through the tissues using a specified beam-waist location and a hyperbolic function to assign beam radius as a function of position. The function $H_0(\lambda,t)$ provides the maximum irradiance per wavelength division at a given time $[W/cm^2/nm]$. The value of $\mu_a(z,\lambda)$ represents the absorption coefficient

$(1/cm)$ at a given wavelength within the tissue, which is determined by the tissue type at the given axial depth, $z[cm]$.

An algorithm which begins with a propagation of an incident laser beam using Equation 7 establishes the irradiance distribution in Equation 9. The algorithm can then use this source term in the solution of Equation 8 for a small time-step, made much smaller than the thermal diffusion time in the material. The algorithm then again propagates the beam through the sample subject to the new refractive index distribution defined by temperature distribution. The alternating solutions then continue for the desired simulation time.

This method provides a basis for the analysis of the effects of thermal lensing. It has the advantage of computing the near-field irradiance distribution, to include aberration effects which occur due to thermal lensing. We have found this method to be an improvement over the first-order Gaussian beam parameter methodologies presented in an earlier paper.[4]

3. RESULTS AND DISCUSSION

Although results to date are somewhat limited, initial predictions show that the numerical models presented are sufficient to provide an exhaustive analysis of propagation effect impact on damage thresholds. The interplay of effects will be complex in many cases, and in the end require an empirical summary to translate the effects to damage thresholds.

3.1. Ultrafast-Pulse Models

Evaluations of Equation 2 were completed as an initial study for the common Ti:Sapphire central wavelength of 810 nm. Simulations were conducted for bandwidth-limited pulses from 20 to 100 fs. Along with input pulses with no bias chirp, calculations were performed with pulses prepared such that they would initially possess a chirp sufficient for GVD compensation to produce a minimal pulse duration at the lens focus for an axial ray. This value of chirp compensation was then searched for a local maximum in the focused-pulse's peak irradiance. Subsequently, the models of Kennedy[12] were applied to the peak irradiance temporal distributions to determine a threshold for LIB.

The resultant analyses of trends in thresholds have been documented in the literature.[3] Figure 3 shows a simplified summary of the results from that study. A reduction to approximately 70 percent of the originally-measured damage threshold was predicted when chirp compensation for GVD effects was included. This reduction was found to decrease to near only 30 percent when the unchirped input pulse duration was 20 fs. Implications for laser safety standards, proposed below the current 100-fs definition, include a much needed complete assessment of propagation effects as a function of chirp condition and wavelength. As exposure limits are often set with roughly a factor of ten margin of safety, it is conceivable that the majority of this margin will be lost for a pre-chirped pulse.

This simple analysis also ignores several other propagation phenomena which will influence the damage threshold. As described by Rockwell[7] and Cain,[3] weak self-focusing or critical self-focusing thresholds may affect sub-picosecond damage thresholds to the retina. In addition, recent research by Vogel[6] implicates the formation of low-density plasmas as a possible mechanism for damage. While the results we have presented in the literature include an earlier LIB model, new theoretical descriptions of the plasma formation thresholds may give additional insight or change predicted trends for damage. Finally, it is well known that super-continuum generation through self-phase modulation can broaden the spectral bandwidth of an infrared laser pulse well into the visible spectrum.[16] This effect may create much lower damage thresholds for the retina from near-infrared pulses, commonly considered to be harmlessly absorbed in the pre-retinal portions of the eye.

3.2. Continuous-Wave Models

In order to validate full-propagation models for continuous-wave beams in the presence of thermal lensing, we have performed a number of time-dependent Z-scan[17] experiments. These provide an method of validating dynamics as well as aberrated beam distributions. Figure 4 illustrates a typical experimental configuration. A Gaussian beam with a TEM_{00} mode is focused through a cuvette of water, and the input beam can be shuttered. The transmitted beam can be monitored in the far-field by two differing methods. The beam profile

distribution can be measured at the detector-aperture plane with a fast-frame-rate camera. This records the far-field, Fresnel-Kirchhoff diffraction pattern from the beam within the sample. As the sample is heated within this beam path, the far-field pattern changes, showing the time-dependent effect of the thermal lens. A second metric within the Z-scan experiment is the measurement of transmittance through an aperture in the far-field. A simple measurement of relative transmittance provides a measure of the beam's distortion in the far field. As thermal lensing takes place, the relative aperture transmittance changes.

Figures 5 and 6 demonstrate typical results from this "closed aperture" Z-scan. When the sample is positioned to the left of the focal position of the beam, a weak thermal-lensing effect will actually increase the transmittance through the far-field aperture. This is due to the fact the negative focal length of the thermal lens moves the focus of the beam toward the aperture, creating a smaller beam at the aperture plane. As the sample moves to the right, the thermal lens caused the beam to broaden at the aperture plane, and we see the transmittance through the aperture decrease as the thermal lens is formed.

The Z-scan data are an excellent construct for examining computational method results. For any given time and sample position combination, the aperture transmittance can be compared to a value computed from the simulated near-field profile as the beam exits the sample, using a Fresnel-Kirchhoff diffraction integral,[18] summed over the area of the experimental aperture. Figure 6 shows a typical comparison of simulation data to experimental data for a fixed-time aperture transmittance as the sample is scanned along the z-axis. We find an excellent agreement between measured an predicted transmittance for both a weak and strong thermal lensing case, with the exception of long times, in which convective flow may distort the beam.

Strong thermal lensing, here, refers to cases in which the far-field pattern observed cannot be approximated by a Gaussian beam profile distribution. Our earlier work[4] demonstrated the limitation of a first-order Gaussian beam parameter paraxial ray-tracing model when strong thermal lensing is present. The finite-difference beam propagation model more accurately mimics the non-Gaussian, far-field beam profile, and can therefore more accurately predict aperture transmittance. This fact is validated through the beam profile evolution measurements captured under the same Z-scan experiment conditions. An example is provided by Figure 7.

Results to date for a complete assessment of the thermal lensing propagation effect on retinal damage thresholds remain somewhat limited. With wavelengths of interest in the 1.2 to 1.4 μm range, limited data are available for the optical properties of the retina. This has made understanding the interplay between thermal lensing and damage thresholds difficult. Multiple solutions exist for possible combinations of absorption coefficient in the retina and chromatic aberrations which result in experimentally-measured damage thresholds.

As a conceptual aid in examining the effects of thermal lensing, a two-layer construct can be used to represent the eye. The anterior (pre-retinal) portions are represented as a single layer with properties of water. The retina and posterior portions are represented by a second layer with differing absorption properties. We have created a version of our model in which an incident Gaussian beam is focused through a Gaussian beam transformation,[19] and the resultant electric field distribution is propagated through the model. Figure 8 illustrates the resultant thermal response along the z-axis of the beam's propagation path. We see that at early times, the temperature rise in the retina layer is much larger than at the anterior portions of the eye. At longer times, the thermal response of the cornea overtakes that of the retina, as the thermal lensing effect decreases the irriadiance level at that position. We have found that as power is varied, as well as the beam diameter at the input, the competing temperature rise can result in first damage in the cornea or the retina. This preliminary result demonstrates that thermal lensing can mediate the position in the eye for damage, and increases the threshold for damage in the retina for dwell times longer than a few tens of microseconds. Although this is only a theoretical construct, recognizing many unknown optical properties in the retina at infrared wavelengths, we have found cases for beam powers of a few watts which cannot damage the retina due to thermal lensing effects, but will damage the cornea after a few seconds. With much higher power, pulses of shorter duration are capable of damaging the retinal layer prior to damaging in the cornea. It is of interest to note that this phenomenon does agree with trends in experimental data presented in the literature.[5]

4. CONCLUSIONS

The role of propagation in the assessment of laser damage thresholds has yet to be completely understood. Regions of the spectrum where moderate absorption occurs are candidates for thermal-lensing influence to the

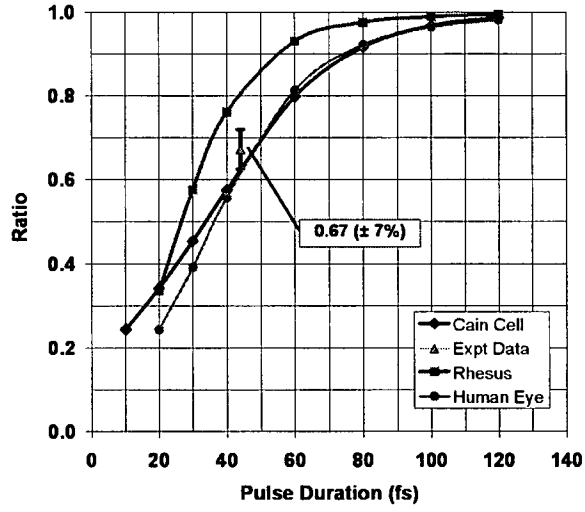

Figure 3. Ratio of pulse-chirp compensation thresholds to those from a transform-limited input pulses. Results are after Cain et al,[3] showing results for an artificial eye cell, as well as aberration-free human and rhesus eye models.

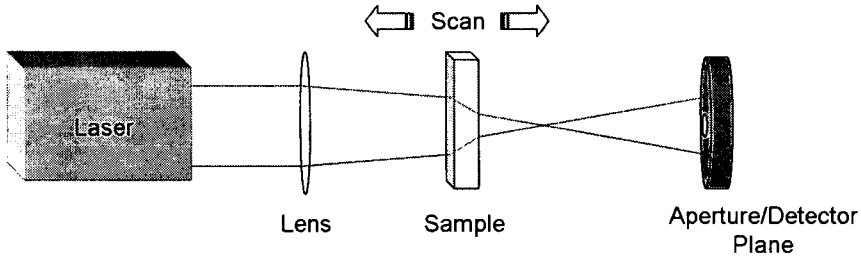

Figure 4. Illustration of a Z-scan experiment setup.

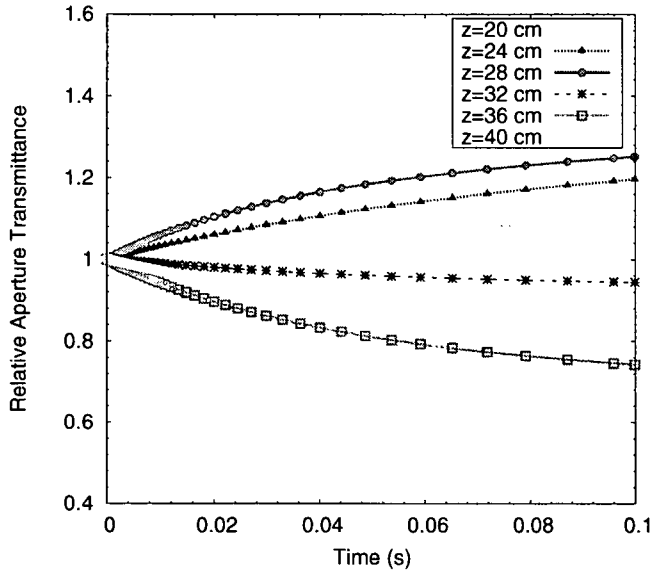

Figure 5. Example of time-dependent Z-scan experimental data for a thermal lensing experiment. The sample is a 2-mm water cell scanned through a focus near 32 cm.

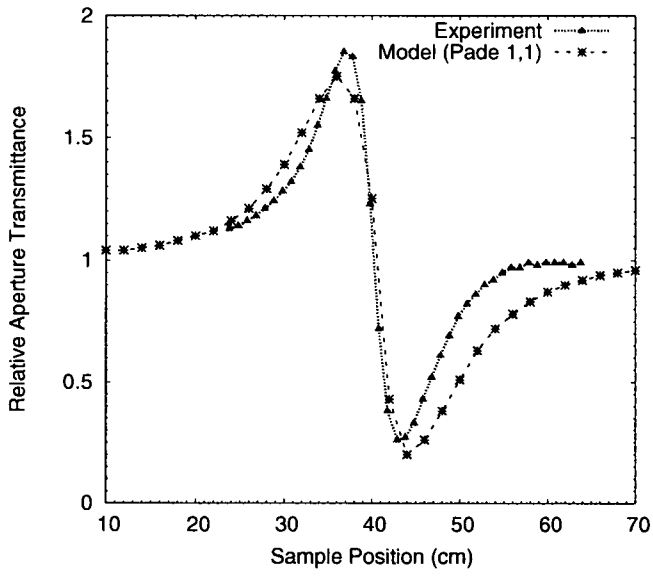

Figure 6. Example of position-dependent Z-scan experimental data compared to computational model results for a thermal lensing experiment. The data correspond to a 1-cm water sample with a focused 48-mW, 1315-nm laser beam.

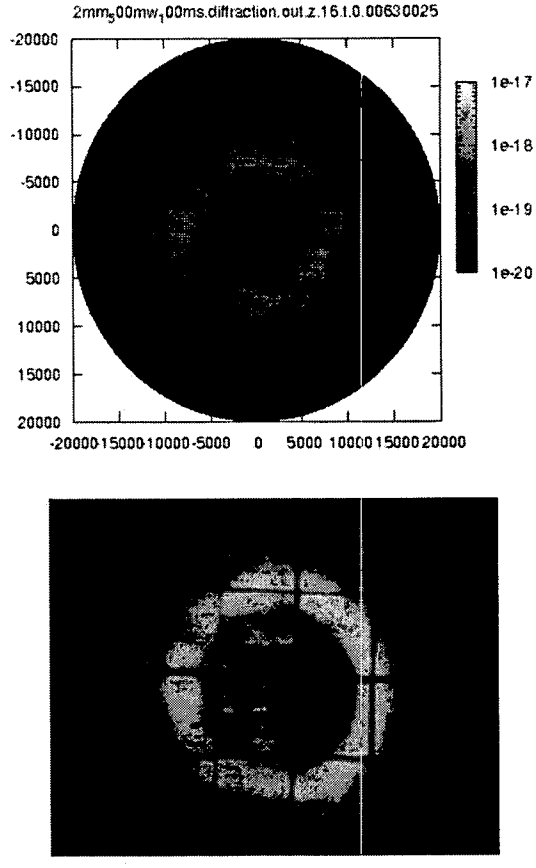

Figure 7. Examples of a far-field diffraction integral irradiance distribution, illustrating the aberrated profile present under strong thermal lensing. The top frame is the result of the computational model, while the lower frame is an experimental result under similar conditions.

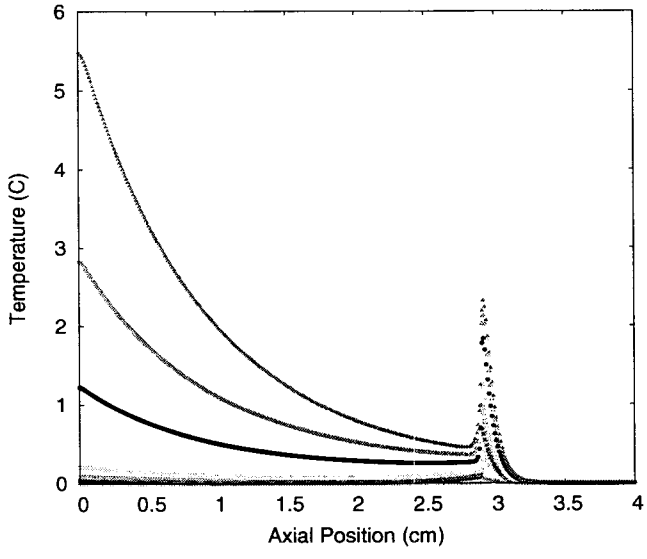

Figure 8. Example of time-dependent thermal response within a two-layer model of the eye for a 3-W beam, and absorption coefficient of 1.7 cm^{-1} in the vitreous.

damage threshold. These thermal-lensing effects, although certainly present, have yet to be investigated fully. Ultrafast pulse propagation, below 100-fs pulse duration, is subject to a variety of linear and non-linear phenomena. The specific hypothesis regarding chirped-pulse compensation, and its influence on retinal damage thresholds, has been validated experimentally.

Acknowledgments

This work was sponsored by the United States Air Force Research Laboratory, and USAF Contract Number F4162402-D-7003. Jacob Stolarski wishes to acknowledge the support of the USAF Research Laboratory Human Effectiveness Directorate Consortium Fellows Program. G.D. Buffington wishes to thank the State of Kansas Biomedical Research Initiative. Opinions expressed here are those of the authors and do not constitute those of the USAF or the Department of Defense.

REFERENCES

1. D. H. Sliney, *Selected Papers on Laser Safety*, SPIE Milestone Series, SPIE, 1987.
2. American National Standards Institute, *Z136.1 American National Standard for Safe Use of Lasers*, Laser Institute of America, Orlando, FL, 2000.
3. C. P. Cain, R. J. Thomas, G. D. Noojin, D. J. Stolarski, P. K. Kennedy, G. D. Buffington, and B. A. Rockwell, "Sub 50-fs laser retinal damage thresholds in primate eyes with group velocity dispersion, self-focusing and low-density plasmas," *Graefe's Archive for Clinical and Experimental Ophthalmology* **243**, pp. 101–112, 2005.
4. R. L. Vincelette, R. J. Thomas, B. A. Rockwell, and A. J. Welch, "A comparison of a first-order thermal lensing model to a closed aperture z-scan for the propagation of light in ocular media.," *Optical Interactions with Tissue and Cells XVII* **6084**(1), p. 60840G, SPIE, 2006.
5. J. A. Zuclich, D. J. Lund, P. R. Edsall, B. E. Stuck, and G. T. Hengst, "High-power lasers in the 1.3- to 1.4-μm wavelength range: ocular effects and safety standard implications," *Laser and Noncoherent Light Ocular Effects: Epidemiology, Prevention, and Treatment* **4246**(1), pp. 78–88, SPIE, 2001.
6. A. Vogel, J. Noack, G. Huettmann, and G. Paltauf, "Femtosecond-laser-produced low-density plasmas in transparent biological media: a tool for the creation of chemical, thermal, and thermomechanical effects below the optical breakdown threshold," *Commercial and Biomedical Applications of Ultrafast and Free-Electron Lasers* **4633**(1), pp. 23–37, SPIE, 2002.
7. B. A. Rockwell, D. J. Payne, R. C. Hopkins, D. X. Hammer, P. K. Kennedy, R. E. Amnotte, B. Eilert, J. J. Druessel, C. A. Toth, W. P. Roach, S. L. Phillips, D. J. Stolarski, G. D. Noojin, R. J. Thomas, and C. P. Cain, "Retinal damage mechanisms from ultrashort laser exposure," *Applications of Ultrashort-Pulse Lasers in Medicine and Biology* **3255**(1), pp. 50–55, SPIE, 1998.
8. D. X. Hammer, A. J. Welch, G. D. Noojin, R. J. Thomas, D. J. Stolarski, and B. A. Rockwell, "Spectrally resolved white-light interferometry for measurement of ocular dispersion," *Journal of the Optical Society of America A* **16**, pp. 2092 - 2102, 1999.
9. E. F. Maher, "Transmission and absorption coefficients for the ocular media of the rhesus monkey," US Army Technical Report SAM-TR-78-32, USAF School of Aerospace Medicine, 1978.
10. C. P. Cain, G. D. Noojin, D. X. Hammer, R. J. Thomas, and B. A. Rockwell, "Artificial eye for in vitro experiments of laser light interaction with aqueous media," *Journal of Biomedical Optics* **2**(1), pp. 88–94, 1997.
11. M. Kempe and W. Rudolph, "Impact of chromatic and spherical aberration on the focusing of ultrashort light pulses by lenses," *Optics Letters* **18**(2), pp. 137–139, 1993.
12. P. K. Kennedy, "A first-order model for computation of laser-induced breakdown thresholds in ocular and aqueous media. I. theory," *IEEE Journal of Quantum Electronics* **31**(12), pp. 2241–2249, 1995.
13. D. I. Kovsh, S. Yang, D. J. Hagan, and E. W. V. Stryland, "Nonlinear optical beam propagation for optical limiting," *Applied Optics* **38**, pp. 5168–5180, 1999.
14. W. H. Press, S. A. Teukolsky, W. T. Vetterling, and B. P. Flannery, *Numerical Recipes in C++, The Art of Scientific Computing*, Cambridge University Press, New York, second ed., 2002.

15. G. R. Hadley, "Wide-angle beam propagation using Pade approximate operators," *Optics Letters* **17**(20), pp. 1426 – 1428, 1992.
16. J. C. Diels and W. Rudolph, *Ultrashort Laser Pulse Phenomena*, Academic Press, New York, 1996.
17. J. Wang, M. Sheik-Bahae, A. A. Said, D. J. Hagan, and E. W. V. Stryland, "Time-resolved z-scan measurements of optical nonlinearities," *JOSA B* **11**(6), pp. 1009–1017, 1994.
18. E. Hecht, *Optics*, Addison-Wesley, 2nd ed., 1987.
19. P. W. Milloni and J. H. Eberly, *Lasers*, John Wiley and Sons, New York, 1998.